processes

MDPI

Article

Targeting GPR55 with Cannabidiol Derivatives: A Molecular Docking Approach Toward Novel Neurotherapeutics

Catalina Mares †, Andra-Maria Paun *, Maria Mernea †, Cristina Matanie and Speranta Avram

Department of Anatomy, Animal Physiology and Biophysics, Faculty of Biology, University of Bucharest, 050095 Bucharest, Romania; catalina.mares@bio.unibuc.ro (C.M.); maria.mernea@bio.unibuc.ro (M.M.); cristina.matanie@bio.unibuc.ro (C.M.); speranta.avram@bio.unibuc.ro (S.A.)

* Correspondence: paun.andra-maria22@s.bio.unibuc.ro

† These authors contributed equally to this work.

Abstract

This study investigated the interaction between cannabidiol (CBD) derivatives and the GPR55 receptor using a bioinformatics-driven molecular docking approach. GPR55, implicated in central nervous system (CNS) pathologies, represents a promising target for novel therapeutics. Drug-likeness evaluation via SwissADME confirmed that all selected derivatives complied with Lipinski's Rule of Five, exhibiting favorable physicochemical properties with molecular weights below 500 Da and acceptable logP values. Molecular docking simulations, performed using AutoDock Vina through PyRx, revealed strong binding affinities, with docking scores ranging from −9.2 to −7.2 kcal/mol, indicating thermodynamically feasible interactions. Visualization and interaction analysis identified a conserved binding pocket involving key residues, including TYR101, PHE102, TYR106, ILE156, PHE169, MET172, TRP177, PRO184, LEU185, LEU270 and MET274. Ligand clustering in this region further supports the presence of a structurally defined binding site. Molecular dynamics simulations of GPR55 in complex with the three top-scoring ligands (3″-HOCBD, THC, and CBL) revealed that all ligands remained stably bound within the cavity over 100 ns, with ligand-specific rearrangements. Predicted oral bioavailability was moderate (0.55), consistent with the need for optimized formulations to enhance systemic absorption. These findings suggest that CBD derivatives may act as potential modulators of GPR55, offering a basis for the development of novel CNS-targeted therapeutics.

Keywords: cannabidiol derivatives; GPR55 receptor; molecular docking; bioinformatics; central nervous system disorders; drug-likeness; SwissADME; binding affinity; phytocompounds

check for updates

Received: 15 September 2025
Revised: 5 October 2025
Accepted: 10 October 2025
Published: 13 October 2025

Citation: Mares, C.; Paun, A.-M.; Mernea, M.; Matanie, C.; Avram, S. Targeting GPR55 with Cannabidiol Derivatives: A Molecular Docking Approach Toward Novel Neurotherapeutics. *Processes* **2025**, *13*, 3261. https://doi.org/10.3390/pr13103261

Copyright: © 2025 by the authors. Licensee MDPI, Basel, Switzerland. This article is an open access article distributed under the terms and conditions of the Creative Commons Attribution (CC BY) license (https://creativecommons.org/licenses/by/4.0/).

1. Introduction

Cannabidiol (CBD) is a natural compound identified in Cannabis sativa [1]. CBD is devoid of psychoactive activity, but studies have shown that it possesses analgesic, anti-inflammatory [2], antineoplastic, and chemopreventive activities, as well as potential therapeutic effects in nervous system disorders such as autism [3], schizophrenia [4], antidepression [5,6], and Alzheimer disease [7]. This plant has been used for thousands of years for recreational, religious and medicinal purposes.

The mechanisms of action of CBD are complex. Although CBD does not produce psychoactive effects [8] and does not appear to bind to specific receptors in the way other compounds might, studies have shown that it can interact with various biological targets [9]. These include ionotropic receptors, nuclear receptors, metabotropic receptors, and enzymes.

These interactions may help explain the wide range of potential medical applications for CBD described in the scientific literature [10].

CBD interacts with multiple targets in the body, and due to the diversity of these targets, it can act as both an agonist and an antagonist, depending on the specific receptor. Studies have also shown that CBD's effects can vary depending on its dose and concentration [9,10].

CBD is a hydrophilic compound, which is rapidly absorbed into adipose tissue and can penetrate the blood–brain barrier, but its bioavailability is very low when administered orally [11].

Numerous studies have investigated the pharmacokinetics and bioavailability of CBD, emphasizing the critical role of both dose and route of administration. Interestingly, a decrease in bioavailability has been observed with increasing CBD doses. Since CBD does not follow a typical absorption pattern and its uptake can be influenced by the dosage form and the individual's nutritional status, the use of CBD-loaded nanoparticles presents a promising strategy to enhance its bioavailability [12–14]. Also, CBD requires special pharmaceutical formulations to be absorbed efficiently.

Based on the observations in the literature on the beneficial effects of CBD on the human body, especially at the level of the central nervous system, we chose to use a bioinformatic approach to the subject. Many pathways of action of this compound are proposed, but the molecular mechanisms are not fully understood and elucidated [7]. However, although it is a potent compound, it has limitations in terms of bioavailability. Unlike Tetrahydrocannabinol (THC), it is not psychoactive and seems to bind to other molecular targets and not to the CB1 and CB2 receptors as expected [15].

However, it can be observed that chronic cannabis use is associated with impairment of cognitive functions, especially memory and executive functions. Studies show that long-term users can experience decreases in IQ, processing speed, and performance on tasks involving verbal memory. Structural changes observed in the hippocampus—a brain region essential for memory—indicate a significant neurobiological impact [16].

Cannabis-derived phytochemicals, particularly CBD and THC, have demonstrated neuroprotective properties relevant to Alzheimer's disease [17]. These compounds act as antioxidants, contributing to the maintenance of synaptic plasticity and the prevention of neuronal loss. Emerging evidence indicates that both CBD and THC enhance the solubility of amyloid-beta peptide (Aβ42) and inhibit the aggregation of Tau protein, two key pathological features of Alzheimer's disease. Despite these promising findings, the full spectrum of their molecular mechanisms remains incompletely understood, highlighting the need for further investigation into their therapeutic potential and pharmacological profiles [18].

Thus, we raise the question: what effects might CBD ingestion have on the brain, and more importantly, how does it interact with neuronal receptors? CBD derivatives may exhibit high affinity for various molecular structures, suggesting significant biological potential.

Given the extensive research on cannabinoid receptors CB1 (CNR1) and CB2 (CNR2), we considered it valuable to include predictions for G protein-coupled receptor 55 (GPR55) as a potential molecular target. GPR55 has been proposed as an alternative or complementary target for cannabidiol (CBD) and its derivatives, and has been associated in the literature with various neuroprotective effects. Its inclusion in the analysis provides a broader perspective on the potential mechanisms of action of these compounds within the central nervous system [19].

GPR55 is expressed in the central nervous system and is often referred to as the 'third cannabinoid receptor' due to its structural and functional relationship with CB1 and CB2. While it appears to play a role in maintaining normal brain function, its precise involvement

in various CNS pathologies remains largely unclear [20]. In the present study, we investigated the potential interaction between CBD derivatives and the GPR55 receptor, aiming to identify novel agonists that may contribute to the modulation of neuroinflammatory processes and exert antidepressant effects [21]. These mechanisms are particularly relevant in the context of neurodegenerative diseases, where inflammation and mood disorders are frequently comorbid [22–24].

In this study, we aim to evaluate the interaction between CBD and its various derivatives identified from scientific databases. Initially, we selected compounds from the scientific literature that are reported to have potential biological roles, as well as derivatives extracted and filtered from the PubChem database [25]. The interaction between cannabidiol (CBD) derivatives and the GPR55 receptor was investigated using in silico approaches [26]. To predict the pharmacological behavior of the selected compounds, molecular modeling techniques were employed. The physicochemical properties and drug-likeness of the compounds were first assessed using the SwissADME platform, while potential molecular targets were identified with SwissTargetPrediction [27]. Molecular docking studies were then conducted to evaluate the binding affinity and interaction patterns of the compounds with GPR55, using AutoDock Vina through the PyRx interface [28]. Since pharmacokinetic parameters play a crucial role in determining the therapeutic potential of drug candidates, ADMET (absorption, distribution, metabolism, excretion, and toxicity) properties were also predicted [29]. Finally, molecular dynamics (MD) simulations were performed on three top scoring ligands to validate and refine the docking results, providing deeper insights into the stability and behavior of the ligand–receptor complexes [30]. Together, these computational strategies represent essential tools in the drug design process, offering a cost-effective and accurate means of prioritizing compounds for further experimental validation.

2. Materials and Methods

2.1. Compounds Identification and Selection

Starting from the main derivatives identified in scientific articles and querying the PubChem database [25] with the keyword "cannabidiol" we obtained a library of compounds. Compounds from PubChem were filtered so that they respected Lipinski's rules [31]. In Table 1 we listed the compounds of interest.

Table 1. Natural compounds, CBD derivatives studied for their effect on the central nervous system.

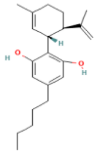
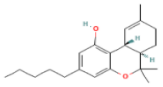
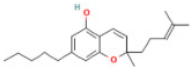
PubChem CID	Molecule Name	2D Structure	Canonical SMILES
644019	CBD		CCCCCC1CC(O)C(C(C1)O)[C@@H]1C=C(C)CC[C@H]1C(=C)C
16078	THC		CCCCCC1=CC(=C2[C@@H]3C=C(CC[C@H]3C(OC2=C1)(C)C)C)O
30219	CBC		CCCCCC1=CC(=C2C=CC(OC2=C1)(C)CCC=C(C)C)O

Table 1. *Cont.*

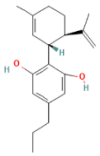
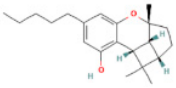
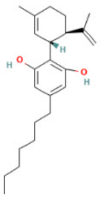
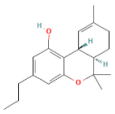
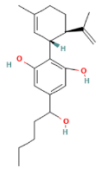
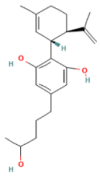
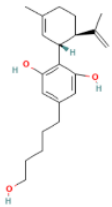
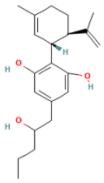
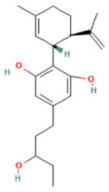
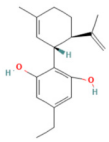
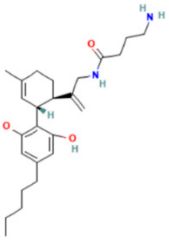
PubChem CID	Molecule Name	2D Structure	Canonical SMILES
11601669	CBDV		CCCC1=CC(=C(C(=C1)O)[C@@H]2C=C(CC[C@H]2C(=C)C)C)O
59444380	CBL		CCCCCC1=CC(=C2[C@@H]3[C@H]4[C@@H](C3(C)C)CC[C@]4(OC2=C1)C)O
49873141	CBDP		CCCCCCCC1=CC(=C(C(=C1)O)[C@@H]2C=C(CC[C@H]2C(=C)C)C)O
93147	THCV		CCCC1=CC(=C2[C@@H]3C=C(CC[C@H]3C(OC2=C1)(C)C)C)O
121596213	1″-HOCBD		CCCCC(C1=CC(=C(C(=C1)O)[C@@H]2C=C(CC[C@H]2C(=C)C)C)O)O
53357352	4″-HOCBD		CC1=C[C@H]([C@@H](CC1)C(=C)C)C2=C(C=C(C=C2O)CCCC(C)O)O
101621543	5″-HOCBD		CC1=C[C@H]([C@@H](CC1)C(=C)C)C2=C(C=C(C=C2O)CCCCCO)O
121596214	2″-HOCBD		CCCC(CC1=CC(=C(C(=C1)O)[C@@H]2C=C(CC[C@H]2C(=C)C)C)O)O
121596215	3″-HOCBD		CCC(CCC1=CC(=C(C(=C1)O)[C@@H]2C=C(CC[C@H]2C(=C)C)C)O)O

Table 1. *Cont.*

PubChem CID	Molecule Name	2D Structure	Canonical SMILES
129210056	CBDE		CCC1=CC(=C(C(=C1)O)[C@@H]2C=C(CC[C@H]2C(=C)C)C)O
44149593	10-((4-Aminobutyryl)amin		CCCCCC1=CC(=C(C(=C1)O)[C@@H]2C=C(CC[C@H]2C(=C)CNC(=O)CCCN)C)O

By querying PubChem [25] using the keyword "cannabidiol", we identified 57 derivative compounds. From these, we selected only those that met the following criteria: clearly defined chemical structure, available experimental or theoretical data on biological activity, scientific relevance in the context of interaction with the nervous system.

2.2. Screening of Biologically Active Molecules

The physicochemical properties of the compounds constitute a critical foundation for elucidating their molecular behavior at the organismal level [32]. These descriptors underpin the rational design of drug candidates. To generate robust and up-to-date predictions based on QSAR models integrated with advanced machine learning algorithms, we utilized the SwissADME platform [33].

Lipinski's Rule of Five is a fundamental guideline in drug design, widely calculated across cheminformatics databases due to its incorporation of key molecular descriptors associated with oral bioavailability. These descriptors include molecular weight, the number of hydrogen bond donors and acceptors, the octanol–water partition coefficient (log P), and the polar surface area (topological polar surface area, TPSA) [31].

2.3. Pharmacokinetics (ADMET) Using Online Database

Furthermore, the pharmacokinetic profiles were characterized using DeepPK [29] enabling a comprehensive evaluation of absorption, distribution, metabolism, and excretion (ADME) parameters [29].

To have a global view on how a drug can actually reach its molecular target, we use Deep Learning algorithms to calculate Absorption, Distribution, Metabolism, Elimination and Toxicity. These algorithms are useful for predicting the ADMET components, but in order to be able to predict each one separately, we selected a series of parameters that we explain later [29].

2.4. Potential Therapeutic Targets

For the prediction of molecular targets, we utilized the SwissTargetPrediction database [34]—an online bioinformatics tool designed to identify potential therapeutic targets of drug-like compounds based on their chemical structure. The platform operates by assessing molecular similarity between the input compound and reference molecules with known bioactivity. By comparing structural features and activity profiles, the tool generates a probability score indicating the likelihood that the tested compound will interact with specific molecular targets [34].

2.5. Molecular Docking Protocol

For the molecular docking studies, we employed PyRx 0.8 software utilizing the AutoDock Vina engine [28]. Protein preparation was carried out using UCSC ChimeraX 1.9 [35]. The target protein structure was retrieved from the RCSB Protein Data Bank (PDB) [36] and processed by removing non-standard residues and water molecules, after which the cleaned structure was saved in .pdb format. Ligands were prepared in .sdf format and subjected to energy minimization using PyRx to ensure optimal conformations for docking. Blind docking was performed across the entire protein surface to identify potential binding sites for the CBD derivatives, as listed in Table 1.

Starting from the crystallographic structure with PDB ID 8ZX5 [23], we used ChimeraX to preprocess the protein by removing heteroatoms and the A, B, and C chains, retaining only the G protein-coupled receptor 55 (GPR55) [23]. This step was essential to isolate the receptor of interest and ensure that the docking results reflect direct interactions between the CBD derivatives and the GPR55 receptor, without interference from additional protein components or ligands present in the original structure [35].

Prior to initiating the molecular docking process, all CBD derivatives listed in Table 1 were imported into PyRx [28] in SDF format via the OpenBabel interface [37]. Each ligand was subjected to energy minimization to obtain optimized conformations. Following minimization, the compounds were converted and saved in .pdbqt format to ensure compatibility with the AutoDock Vina docking protocol [38,39].

Using the Vina Wizard interface within PyRx [28], the previously processed GPR55 [23] protein structure was imported and automatically converted into the .pdbqt format required for molecular docking. This ensured compatibility with the AutoDock Vina engine and allowed for seamless integration into the docking workflow.

Discovery Studio Visualizer 24.1.0.23298 [40] identified the presence of eight possible binding sites from receptor cavities, outlined with differently colored dots in Figure 1a. The volume of these cavities ranges from 624 $Å^3$ (red dots) to 12.5 $Å^3$ (yellow dots). Although the largest cavity accommodates the AM251 ligand in 8ZX5 structure [23] and molecular docking studies typically focus on the active site [41], in our analysis we decided to investigate which of the identified cavities exhibits the highest binding affinity for the selected ligands [42]. Blind molecular docking was performed using AutoDock Vina 1.2.0 within the PyRx platform. The docking grid was defined to encompass the entire GPR55 protein structure, allowing for an unbiased search of potential binding sites. The grid box was centered at coordinates X: 11.0138, Y: 106.2756, Z: 90.3624, with dimensions (in Ångströms) of X: 37.3478, Y: 59.0478, and Z: 62.0155.

For data visualization and interaction analysis, we employed Discovery Studio Visualizer [40] to examine the molecular interactions between the GPR55 receptor and selected CBD derivatives. This step was essential for identifying the potential binding pocket at the receptor level. High binding affinity, as observed in our docking studies, may indicate a likely active site on the receptor. GPR55 is a receptor of growing interest due to its involvement in various pathological conditions, including cancer, neurodegenerative diseases, depression, and anxiety. Therefore, identifying potential ligands capable of modulating GPR55 activity is of significant importance for future therapeutic development.

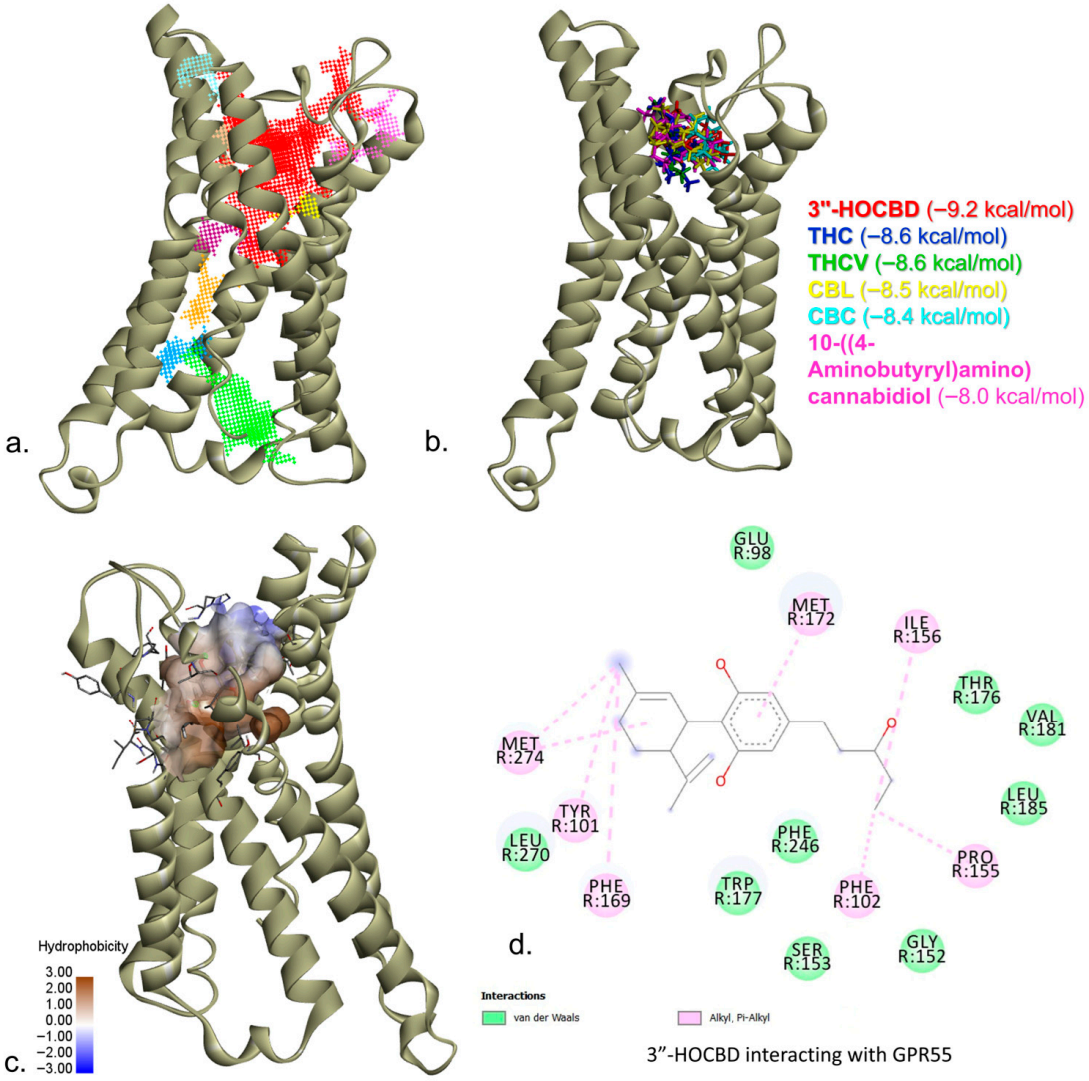


Figure 1. (**a**) Predicted binding cavities of GPR55 receptor. The dots line the identified cavities volumes, each color marking a different cavity. (**b**) Superimposed representations of selected top-ranked ligand binding poses in the receptor. The inset shows the correspondence between ligands, their colors, and docking affinities. (**c**) Representation of 3″-HOCBD predicted binding pocket. The pocket surface was colored according to hydrophobicity based on a brown to blue scale, as shown in the insert. (**d**) 2D interaction map derived for the best pose of 3″-HOCBD bound in GPR55 cavity. The association between colors and interaction types is shown in the insert. All images were obtained using Discovery Studio Visualizer [40].

2.6. Molecular Dynamics

Molecular dynamics (MD) simulations were performed using NAMD 3.0.2 [43]. CHARMM force field family [44] was employed, with protein parameters from CHARMM36m [45], lipid parameters from CHARMM36 [46] and ligand parameters derived from the CHARMM General Force Field [47]. The ligand parameters of 3″-HOCBD, THC and CBL were estimated based on CHARMM General Force Field [47] using CHARMM-Gui Ligand Reader & Modeler module [48,49].

Each protein—ligand complex (GPR55—3″-HOCBD, GPR55—THC and GPR55—CBL) was embedded in a POPC (1-palmitoyl-2-oleoyl-glycero-3-phosphocholine) lipid bilayer (~6400 Å^2) and solvated with 20 Å of water molecules on both sides. Na^+ and Cl^- ions were added to neutralize the system and reach 150 mM NaCl. System preparation was performed using CHARMM-Gui Membrane Builder [49,50].

The energy minimization and equilibration of simulation systems were performed following the standard CHARMM-Gui Membrane Builder protocol [51]. The system underwent energy minimization, followed by a six-step equilibration procedure with gradually decreasing positional restraints on protein, lipids, and solvent, allowing progressive relaxation of the system to the target temperature (300 K) and pressure (1 atm) under NPT ensemble conditions.

Production MD simulations at 300 K and 1 atm (NPT ensemble) were then performed for 100 ns per system. Simulations employed a 2 fs timestep, with all bonds involving hydrogen constrained. Nonbonded interactions were calculated every step with a 12 Å cutoff, and long-range electrostatics were treated using particle mesh Ewald (PME) with 6th-order spline interpolation and 1 Å grid spacing. All molecules were wrapped to the simulation cell using periodic boundary conditions.

The analysis of MD trajectories to assess ligand stability was performed using VMD version 1.9.4a12 [52]. Protein and ligand dynamics were analyzed from the MD trajectories after aligning all frames to the protein backbone of the reference structure, defined as the final frame of the equilibration prior to the production run. Analyses included root mean squared deviation (RMSD) time series of the protein backbone to assess overall structural stability, root mean squared fluctuations (RMSF) of protein residues to evaluate local flexibility, and RMSD of the ligands to monitor their conformational stability within the binding site. Additionally, the distance between the ligand center of mass (COM) in each frame and the COM of the ligand in the reference structure was calculated to track ligand displacement. Ligand–protein contacts were quantified as the number of protein atoms located within 5 Å of the ligand throughout the simulation.

3. Results

3.1. Molecular Properties and DrugLike Rules

The biological derivatives of CBD were evaluated using the SwissADME [33] database to assess their physicochemical properties and their compliance with established drug-likeness criteria. These compounds were selected from the PubChem database [25] by applying molecular weight filters, ensuring that all analyzed derivatives meet the criterion of having a molecular weight (MW) below 500 Da [28].

As shown in Table 2, the properties relevant to Lipinski's rule of five were calculated for both CBD and its derivatives, with a particular focus on the Consensus LogP value. This parameter represents the octanol–water partition coefficient, an indicator of lipophilicity. Values above 5 are generally considered violations of Lipinski's rule, suggesting potentially poor absorption or permeation [53].

Although Lipinski's rule of five is the most widely used guideline in drug design, the SwissADME database enables the evaluation of additional important rules relevant to this process [31,33]. This comprehensive analysis allows for a comparative overview of the main drug-likeness criteria described in the literature.

As presented in Table 3, certain compounds exhibit violations of these supplementary rules, indicating potential limitations in their drug-like behavior. Furthermore, the database provides an estimate of the bioavailability score, which in this case is moderate, with a value of 0.55.

Table 2. Properties of CBD derivatives predicted with SwissADME [33].

Molecule	MW	#H-Bond Acceptors	#H-Bond Donors	TPSA	Consensus Log P
CBD	314.46	2	2	40.46	5.2
THC	314.46	2	1	29.46	5.33
CBC	314.46	2	1	29.46	5.45
CBDV	286.41	2	2	40.46	4.5
CBL	314.46	2	1	29.46	5.08
CBDP	342.51	2	2	40.46	5.92
THCV	286.41	2	1	29.46	4.68
1″-HOCBD	330.46	3	3	60.69	4.41
4″-HOCBD	330.46	3	3	60.69	4.3
5″-HOCBD	330.46	3	3	60.69	4.34
2″-HOCBD	330.46	3	3	60.69	4.26
3″-HOCBD	330.46	3	3	60.69	4.27
CBDE	272.38	2	2	40.46	4.17
10-((4-Aminobutyryl)amino) cannabidiol	414.58	4	4	95.58	4.18

Table 3. Drug Design rules predicted using SwissADME [33].

Molecule	Lipinski #Violations	Ghose #Violations	Veber #Violations	Egan #Violations	Muegge #Violations	Bioavailability Score
CBD	1	1	0	0	1	0.55
THC	1	1	0	0	1	0.55
CBC	1	1	0	1	1	0.55
CBDV	0	0	0	0	1	0.55
CBL	1	0	0	0	1	0.55
CBDP	1	1	0	1	1	0.55
THCV	0	0	0	0	1	0.55
1″-HOCBD	0	0	0	0	1	0.55
4″-HOCBD	0	0	0	0	0	0.55
5″-HOCBD	0	0	0	0	0	0.55
2″-HOCBD	0	0	0	0	0	0.55
3″-HOCBD	0	0	0	0	0	0.55
CBDE	0	0	0	0	0	0.55
10-((4-Aminobutyryl) amino)cannabidiol	0	0	1	0	0	0.55

3.2. Pharmacokinetics

Absorption, as presented in Table 4, is a critical characteristic to evaluate when developing potential future drugs. Based on literature reports highlighting the limited absorption of CBD and the need for specialized pharmaceutical formulations to enhance its bioavailability, we estimated the absorption levels of compounds structurally similar to CBD.

3.2.1. Absorption

Absorption can be estimated using different items. In the case of the compounds in the list, the absorption and oral bioavailability and the level of confidence in the model can be estimated using the DeepPK tool [29].

Absorption, as presented in Table 4, is a critical characteristic to evaluate when developing potential future drugs. Based on literature reports highlighting the limited absorption of CBD and the need for specialized pharmaceutical formulations to enhance its bioavailability, we estimated the absorption levels of compounds structurally similar to CBD.

Table 4. Absorption of CBD derivatives used DeepPK tool [29]. Specifically, we can see that all compounds in the series are absorbed and show a high degree of confidence in the prediction.

Compound Name	Human Oral Bioavailability 20% Probability	Human Oral Bioavailability 50% Probability	Human Intestinal Absorption Probability	Human Intestinal Absorption Interpretation
CBD	0.57	0.337	0.985	Absorbed (High Confidence)
THC	0.674	0.41	0.994	Absorbed (High Confidence)
CBC	0.621	0.53	0.992	Absorbed (High Confidence)
CBDV	0.712	0.405	0.994	Absorbed (High Confidence)
CBDV	0.712	0.405	0.994	Absorbed (High Confidence)
CBDP	0.516	0.327	0.987	Absorbed (High Confidence)
THCV	0.757	0.461	0.997	Absorbed (High Confidence)
1″-HOCBD	0.56	0.365	0.983	Absorbed (High Confidence)
4″-HOCBD	0.676	0.337	0.989	Absorbed (High Confidence)
5″-HOCBD	0.57	0.337	0.985	Absorbed (High Confidence)
2″-HOCBD	0.607	0.38	0.984	Absorbed (High Confidence)
3″-HOCBD	0.633	0.386	0.985	Absorbed (High Confidence)
CBDE	0.745	0.432	0.994	Absorbed (High Confidence)
10-((4-Aminobutyryl) amino)cannabidiol	0.412	0.325	0.971	Absorbed (High Confidence)

3.2.2. Distribution

Distribution, shown in Table 5, represents the ability of compounds to cross physiological barriers of the organism. In this case we are looking at the ability of CBD and its derivatives to cross the central nervous system and the blood–brain barrier. Thus, in order to build drugs for the central nervous system, it is absolutely necessary for these compounds to cross the BBB.

Table 5. Distribution of CBD derivatives used DeepPK tool [29].

Compound Name	Central Nervous System Predictions	Blood–Brain Barrier Probability
CBD	−2.13	0.793
THC	−2.53	0.998
CBC	−2.29	0.981
CBDV	−2.2	0.983
CBDV	−2.2	0.983
CBDP	−1.96	0.984
THCV	−2.62	0.997
1″-HOCBD	−2.14	0.841
4″-HOCBD	−2.31	0.797
5″-HOCBD	−2.13	0.793

Table 5. *Cont.*

Compound Name	Central Nervous System Predictions	Blood–Brain Barrier Probability
2″-HOCBD	−2.09	0.691
3″-HOCBD	−2.24	0.545
CBDE	−2.2	0.989
10-((4-Aminobutyryl) amino)cannabidiol	−2.19	0.91

3.2.3. Metabolism

Using the DeepPk [29] database (https://biosig.lab.uq.edu.au/deeppk/, accessed on 9 October 2025), we predicted the potential of these compounds to act as inhibitors or substrates of the major cytochrome P450 isoforms. The corresponding results are summarized in Table 6.

Table 6. Metabolism of CBD derivatives probability.

Compound Name	CYP 1A2 Inhibitor	CYP 1A2 Substrate	CYP 2C19 Inhibitor	CYP 2C19 Substrate	CYP 2C9 Inhibitor	CYP 2C9 Substrate	CYP 2D6 Inhibitor	CYP 2D6 Substrate	CYP 3A4 Inhibitor	CYP 3A4 Substrate
CBD	0.942	0.379	0.523	0.595	0.882	0.767	0.179	0.419	0.927	0.518
THC	0.995	0.599	0.963	0.634	0.986	0.974	0.32	0.567	0.732	0.756
CBC	0.931	0.539	0.883	0.604	0.659	0.975	0.917	0.578	0.637	0.808
CBDV	0.874	0.466	0.984	0.608	0.969	0.959	0.867	0.474	0.865	0.631
CBDV	0.874	0.466	0.984	0.608	0.969	0.959	0.867	0.474	0.865	0.631
CBDP	0.977	0.359	0.91	0.612	0.881	0.818	0.652	0.428	0.891	0.626
THCV	0.992	0.669	0.981	0.615	0.981	0.984	0.928	0.568	0.668	0.712
1″-HOCBD	0.821	0.307	0.896	0.619	0.951	0.884	0.287	0.397	0.856	0.404
4″-HOCBD	0.904	0.356	0.784	0.612	0.801	0.846	0.01	0.457	0.861	0.484
5″-HOCBD	0.942	0.379	0.523	0.595	0.882	0.767	0.179	0.419	0.927	0.518
2″-HOCBD	0.799	0.317	0.923	0.623	0.891	0.864	0.277	0.419	0.867	0.429
3″-HOCBD	0.835	0.328	0.861	0.613	0.768	0.849	0.012	0.415	0.816	0.45
CBDE	0.722	0.485	0.985	0.604	0.947	0.964	0.689	0.483	0.792	0.624
10-((4-Amin obutyryl)amino) cannabidiol	0.658	0.195	0.664	0.626	0.629	0.098	0.985	0.436	0.956	0.294

Although the analyzed compounds exhibit only minor structural variations, primarily involving the positional rearrangement of atoms, these similarities are reflected in their predicted interactions with cytochrome P450 isoforms. As shown in Table 6, the CBD derivatives demonstrate a high probability of acting as inhibitors of CYP1A2, CYP2C19, CYP2C9, and CYP3A4. Additionally, it is noteworthy that these compounds are also predicted to serve as substrates for CYP2C9, suggesting a potential role in metabolic processing via this isoform.

3.2.4. Excretion

Table 7 summarizes the predicted excretion profiles of potential CBD derivatives, indicating their roles as inhibitors or substrates of the OCT2 transporter. Additionally, the estimated half-life of each compound is analyzed to provide insight into their elimination kinetics.

The results indicate that neither CBD nor its derivatives act as inhibitors of OCT2, suggesting efficient renal elimination of these compounds. Furthermore, the predicted half-life of the CBD derivatives is under 3 hs. This parameter is important to monitor, as an ideal therapeutic compound should be effectively cleared to avoid accumulation and potential toxicity in the body.

Table 7. Excretion of CBD derivatives.

Compound Name	Organic Cation Transporter 2 Probability	Organic Cation Transporter 2 Interpretation	Half-Life of Drug Predictions	Half-Life of Drug Probability	Half-Life of Drug Interpretation
CBD	0.382	Non-Inhibitor (Low Confidence)	Half-Life < 3 hs	0.243	Half-Life < 3 hs (Medium Confidence)
THC	0.394	Non-Inhibitor (Low Confidence)	Half-Life < 3 hs	0.135	Half-Life < 3 hs (High Confidence)
CBC	0.322	Non-Inhibitor (Medium Confidence)	Half-Life < 3 hs	0.178	Half-Life < 3 hs (Medium Confidence)
CBDV	0.307	Non-Inhibitor (Medium Confidence)	Half-Life < 3 hs	0.243	Half-Life < 3 hs (Medium Confidence)
CBDV	0.307	Non-Inhibitor (Medium Confidence)	Half-Life < 3 hs	0.243	Half-Life < 3 hs (Medium Confidence)
CBDP	0.358	Non-Inhibitor (Low Confidence)	Half-Life < 3 hs	0.206	Half-Life < 3 hs (Medium Confidence)
THCV	0.425	Non-Inhibitor (Low Confidence)	Half-Life < 3 hs	0.157	Half-Life < 3 hs (High Confidence)
1″-HOCBD	0.263	Non-Inhibitor (Medium Confidence)	Half-Life < 3 hs	0.319	Half-Life < 3 hs (Medium Confidence)
4″-HOCBD	0.326	Non-Inhibitor (Medium Confidence)	Half-Life < 3 hs	0.234	Half-Life < 3 hs (Medium Confidence)
5″-HOCBD	0.382	Non-Inhibitor (Low Confidence)	Half-Life < 3 hs	0.243	Half-Life < 3 hs (Medium Confidence)
2″-HOCBD	0.269	Non-Inhibitor (Medium Confidence)	Half-Life < 3 hs	0.314	Half-Life < 3 hs (Medium Confidence)
3″-HOCBD	0.313	Non-Inhibitor (Medium Confidence)	Half-Life < 3 hs	0.252	Half-Life < 3 hs (Medium Confidence)
CBDE	0.266	Non-Inhibitor (Medium Confidence)	Half-Life < 3 hs	0.255	Half-Life < 3 hs (Medium Confidence)
10-((4-Aminobutyryl) amino)cannabidiol	0.407	Non-Inhibitor (Low Confidence)	Half-Life < 3 hs	0.297	Half-Life < 3 hs (Medium Confidence)

3.2.5. Toxicity

The predicted toxicity profiles of the CBD derivatives are presented in Table 8. Most compounds in the series are generally classified as safe with respect to AMES mutagenicity, hepatotoxicity, and cardiotoxicity. However, according to data obtained from the DeepPK database [29], both CBD and its hydroxy derivatives exhibit a potential risk of cardiotoxicity, likely due to predicted hERG channel inhibition. Notably, the compound 10-((4-Aminobutyryl)amino)cannabidiol demonstrates significant cardiotoxic potential through hERG inhibition, suggesting that it may not be a suitable candidate for further drug development.

Table 8. Toxicity of CBD derivatives used DeepPk [29].

Compound Name	AMES Mutagenesis	Carcinogenesis	Liver Injury I (DILI)	Liver Injury II	hERG Blockers
CBD	Safe	Toxic	Safe	Safe	Safe
THC	Safe	Safe	Safe	Toxic	Safe
CBC	Safe	Safe	Safe	Safe	Safe
CBDV	Safe	Safe	Safe	Safe	Safe
CBDV	Safe	Safe	Safe	Safe	Safe
CBDP	Safe	Toxic	Safe	Safe	Safe
THCV	Safe	Safe	Safe	Toxic	Safe
1″-HOCBD	Safe	Safe	Safe	Safe	Safe
4″-HOCBD	Safe	Toxic	Safe	Safe	Safe
5″-HOCBD	Safe	Toxic	Safe	Safe	Safe
2″-HOCBD	Safe	Toxic	Safe	Safe	Safe
3″-HOCBD	Safe	Toxic	Safe	Safe	Safe
CBDE	Safe	Safe	Safe	Safe	Safe
10-((4-Aminobutyryl)amino)cannabidiol	Safe	Toxic	Safe	Toxic	Toxic

3.3. Pharmacodynamics

Table 9 presents the predicted molecular targets for CBD derivatives, based on SwissTargetPrediction analysis [34]. Among the most prominent targets identified are Cannabinoid Receptor 1 (CNR1) and Cannabinoid Receptor 2 (CNR2), both displaying high interaction probabilities exceeding 0.85. In addition to these classical cannabinoid receptors, G protein-coupled receptor 55 (GPR55) was also predicted as a likely target, showing a similarly high probability of interaction. Notably, the literature highlights distinct pharmacological profiles for CBD and THC: while THC is associated with psychoactive effects

and is commonly used for recreational purposes, CBD is characterized by a lack of psychoactivity. Consistent with these findings, Table 9 reveals a difference of approximately 6 percentage points in predicted affinity between CBD and THC for CNR1 and CNR2, with THC demonstrating a higher binding probability to both receptors.

Table 9. Molecular targets of CBD derivates from SwissTargetPrediction tool [34].

Target	Common Name	Target Class	Probability
CBD			
Cannabinoid receptor 1	CNR1	Family A G protein-coupled receptor	0.893165
Cannabinoid receptor 2	CNR2	Family A G protein-coupled receptor	0.893165
G-protein coupled receptor 55	GPR55	Family A G protein-coupled receptor	0.818184
THC			
Cannabinoid receptor 1	CNR1	Family A G protein-coupled receptor	0.959682
N-arachidonyl glycine receptor	GPR18	Family A G protein-coupled receptor	0.959682
Cannabinoid receptor 2	CNR2	Family A G protein-coupled receptor	0.959682
Glycine receptor subunit alpha-1	GLRA1	Ligand-gated ion channel	0.959682
CBC			
Cannabinoid receptor 1	CNR1	Family A G protein-coupled receptor	0.959682
N-arachidonyl glycine receptor	GPR18	Family A G protein-coupled receptor	0.959682
Cannabinoid receptor 2	CNR2	Family A G protein-coupled receptor	0.959682
Glycine receptor subunit alpha-1	GLRA1	Ligand-gated ion channel	0.959682
CBDV			
Cannabinoid receptor 1	CNR1	Family A G protein-coupled receptor	0.897728
Cannabinoid receptor 2	CNR2	Family A G protein-coupled receptor	0.897728
G-protein coupled receptor 55	GPR55	Family A G protein-coupled receptor	0.641391
CBL			
Cannabinoid receptor 1	CNR1	Family A G protein-coupled receptor	0.693215
Cannabinoid receptor 2	CNR2	Family A G protein-coupled receptor	0.693215
CBDP			
Cannabinoid receptor 1	CNR1	Family A G protein-coupled receptor	0.825425
Cannabinoid receptor 2	CNR2	Family A G protein-coupled receptor	0.825425
G-protein coupled receptor 55	GPR55	Family A G protein-coupled receptor	0.758299
THCV			
Cannabinoid receptor 1	CNR1	Family A G protein-coupled receptor	0.906315
N-arachidonyl glycine receptor	GPR18	Family A G protein-coupled receptor	0.786927
Cannabinoid receptor 2	CNR2	Family A G protein-coupled receptor	0.786927
Glycine receptor subunit alpha-1	GLRA1	Ligand-gated ion channel	0.786927
Vascular endothelial growth factor receptor 2	KDR	Kinase	0.542516
1″-HOCBD			
Cannabinoid receptor 1	CNR1	Family A G protein-coupled receptor	0.371182
Cannabinoid receptor 2	CNR2	Family A G protein-coupled receptor	0.371182
4″-HOCBD			
Cannabinoid receptor 1	CNR1	Family A G protein-coupled receptor	0.573001
Cannabinoid receptor 2	CNR2	Family A G protein-coupled receptor	0.573001
5″-Hydroxycannabidiol			
Cannabinoid receptor 1	CNR1	Family A G protein-coupled receptor	0.613334
2″-HOCBD			
Cannabinoid receptor 1	CNR1	Family A G protein-coupled receptor	0.459956
Cannabinoid receptor 2	CNR2	Family A G protein-coupled receptor	0.459956
3″-HOCBD			
Cannabinoid receptor 1	CNR1	Family A G protein-coupled receptor	0.629642
Cannabinoid receptor 2	CNR2	Family A G protein-coupled receptor	0.629642
CBDE			
Cannabinoid receptor 1	CNR1	Family A G protein-coupled receptor	0.608509
Cannabinoid receptor 2	CNR2	Family A G protein-coupled receptor	0.608509
10-((4-Aminobutyryl)amino)cannabidiol			
Cannabinoid receptor 2	CNR2	Family A G protein-coupled receptor	0.106166

Particular attention should be given to the GPR55 receptor, which shares several cannabinoid ligands with CB1 and CB2, despite being structurally distinct. Notably, high binding affinities have been predicted between GPR55 and several CBD derivatives, suggesting a potential pharmacological relevance. To further validate these findings, we will perform molecular docking studies to explore the specific interactions between GPR55 and the CBD derivatives listed in Table 1.

3.4. Molecular Docking

Following molecular docking using PyRx and AutoDock Vina [28,38], we obtained promising binding affinity results. The ligands demonstrated favorable interactions with the GPR55 receptor, with binding energies ranging from −9.2 to −6.8 kcal/mol.

Table 10 presents the ligands that exhibited the strongest binding affinity with the GPR55 receptor (PDB ID: 8ZX5) [23]. The most favorable binding affinity of −9.2 kcal/mol was obtained for 3″-HOCBD. A high biding affinity was also obtained

for THC (−8.6 kcal/mol). In addition, the ligands associated with the top ranked poses include THCV, CBL, CBC, and 10-((4-Aminobutyryl)amino)cannabidiol (Figure 1b).

Table 10. The results obtained from the molecular docking protocol using PyRx and AutoDock Vina [28] filtered based on the most favorable binding affinities. The names of the molecules are abbreviated according to Table 1. The ligand codes were assigned by PyRx, comprising the name of the PDB structure used for docking (8zx5), followed by the compound CID from PubChem (see Table 1), the force field used for energy minimization (here uff—Universal Force Field) and the calculated internal energy of the ligand after minimization, expressed in kcal/mol.

Molecule Name	Ligand	Beste Pose Binding Affinity (kcal/mol)	Interacting Aminoacids
3″-HOCBD	8zx5_121596213_uff_E = 233.98	−9.2	TYR101, PHE102, PRO 155, ILE 156,PHE 169, MET 172, MET274
THC	8zx5_16078_uff_E = 312.91	−8.6	HIS27, LEU77, LYS80, TYR 101, PHE 169, TRP177, MET172,LEU270, MET274
THCV	8zx5_93147_uff_E = 308.78	−8.6	HIS27, LYS80, TYR101, MET172, PHE169, TRP177, LEU 270, MET 274
CBL	8zx5_59444380_uff_E = 965.10	−8.5	TYR 101, PHE 169, LEU270, MET274
CBC	8zx5_30219_uff_E = 202.54	−8.4	PHE102, PRO155,ILE156, LEU185, PHE169, MET 172
10-((4-Aminobutyryl) amino)cannabidiol	8zx5_44149593_uff_E = 278.31	−8	TYR101, PHE169, MET172, TRP 177, PHE 246, LEU 270 MET 274, GLN 271
4″-HOCBD	8zx5_53357352_uff_E = 242.61	−7.8	PHE 102, ILE 156, PHE 169, LEU270, MET 274
5″-HOCBD	8zx5_101621543_uff_E = 233.63	−7.7	LYS80, TYR101, PHE169, HIS170, MET 172, MET274
CBDP	8zx5_49873141_uff_E = 221.20	−7.6	TYR101, PHE102, ILE 156, PHE169, MET172, LEU185, PHE 246, LEU270, MET274
CBDV	8zx5_11601669_uff_E = 309.11	−7.6	HIS27, LYS80, TYR101, PHE169, MET172, PHE246, MET274
1″-HOCBD	8zx5_121596213_uff_E = 214.48	−7.5	TYR101, PHE102, ILE156, MET172, TRP 177, LEU270
2″-HOCBD	8zx5_121596214_uff_E = 242.42	−7.5	GLN23, TYR101, PHE102, ILE156, MET172, HIS170, PHE169, LEU270, GLN271, MET274
CBD	8zx5_644019_uff_E = 254.46	−7.3	TYR101, PHE 102, ILE156, PHE169, MET172, LEU270, MET274
CBDE	8zx5_129210056_uff_E = 205.71	−7.2	TYR101, PHE169 MET172, ILE156, TRP177, LEU270

Although molecular docking was performed blindly across the entire protein surface, the ligands were observed to cluster within a specific binding pocket, which represents the main receptor pocket, as shown in Figure 1a,b. The ligands represented in Figure 1b are those with the most favorable binding affinity scores. This observation aligns with the QSAR (Quantitative Structure–Activity Relationship) principle, which suggests that structurally similar compounds are likely to exhibit similar biological activities [54]. In the context of molecular docking, such structural similarity often results in binding at the same or overlapping amino acid residues, thereby supporting the identification of a consistent and potentially biologically relevant binding pocket.

To gain deeper insight into the molecular interactions, we used Discovery Studio Visualizer [40] to identify the amino acid residues involved in ligand binding and to characterize the architecture of the binding pocket. In the case of the highest-scoring ligand 3″-HOCBD, we depicted the surface of its binding site in Figure 1c, showing that the pocket is mostly hydrophobic. The detailed 2D interaction map of 3″-HOCBD with the receptor (Figure 1d) shows that the ligand forms alkyl and pi-alkyl interactions with residues TYR101, PHE102, PRO155, ILE156, PHE169, MET172 and MET274 and van der Waals interactions with residues GLU98, GLY152, SER153, THR176, TRP177, VAL181, LEU185, PHE246 and LEU270.

Complete 2D interaction diagrams of all docked compounds are provided in Supplementary Materials (Figure S1). These diagrams show that the ligands occupy different regions within the binding cavity, yet share a consistent interaction pattern with a common set of residues in a specific binding region. Several amino acid residues— TYR101, PHE102, TYR106, ILE156, PHE169, MET172, TRP177, PRO184, LEU185, LEU270 and MET274—appear repeatedly across multiple ligand-receptor complexes. The recurrent presence of these residues suggests the existence of a conserved binding pocket at the receptor level. Aromatic and hydrophobic residues such as PHE, TYR, and TRP may contribute significantly to ligand stabilization through π–π interactions and hydrophobic contacts. These

findings support the idea that this pocket may represent a pharmacologically relevant site for modulating GPR55 activity, offering a structural basis for further in silico and in vitro investigations of CBD derivatives.

3.5. MD Simulations

Molecular dynamics (MD) simulations were performed to evaluate the stability of the top-scoring ligands within the GPR55 binding pocket. Specifically, we selected the two highest-scoring compounds, 3″-HOCBD and THC, and, given the structural similarity between THCV and THC, we additionally included CBL for MD simulation. For each complex between GPR55 and the ligands 3″-HOCBD, THC and CBL we simulated 100 ns of MD.

3.5.1. Receptor Dynamics in the Protein—Ligand Complexes

The protein backbone RMSD time series (Figure 2a) indicates that the protein undergoes structural adjustments to accommodate the ligand during the first 50 ns of simulation. After this equilibration period, all systems reach a quasi-stable state, with mean RMSD values of 2.15 ± 0.13 Å for the 3″-HOCBD system, 2.36 ± 0.14 Å for the THC system, and 2.94 ± 0.15 Å for the CBL system relative to the structure after the equilibration steps (Figure 2a). These results suggest that the protein remained most stable in complex with 3″-HOCBD, whereas CBL binding induced more pronounced conformational rearrangements. The RMSF plot in Figure 2b indicates that the protein backbone exhibits a broadly similar fluctuation pattern across all three complexes, with the most flexible regions largely conserved. However, subtle differences in residue flexibility are observed. For example, in the GPR55–THC complex, residues ASP70–PHE110 display reduced flexibility compared to the other complexes. Conversely, residues PHE120–GLY140 are more flexible in the GPR55–CBL complex relative to the others. These variations suggest that the ligand type can influence local protein dynamics within otherwise conserved flexible regions. Regarding the ligand binding sites identified in Section 3.4 (residues TYR101, PHE102, TYR106, ILE156, PHE169, MET172, TRP177, PRO184, LEU185, LEU270, and MET274), Figure 2b shows ligand-dependent differences in residue flexibility. Notably, TYR101, PHE102, and TYR106 exhibit higher fluctuations in the GPR55–CBL complex. In general, most binding site residues display increased flexibility in the presence of CBL, suggesting that the binding site undergoes larger structural rearrangements to accommodate this ligand.

3.5.2. Ligand Dynamics in the Protein—Ligand Complexes

The structures of GPR55 complexes with the three ligands at the beginning and at the end of the MD simulations are shown in Figure 3. Ligands remain within the same binding cavity, although they exhibit different degrees of reorientation: smaller for 3″-HOCBD and larger for THC. To quantify ligand dynamics, we first calculated RMSD time series relative to the equilibrated structure at the start of the production MD run (Figure 4a). The RMSD plots show stabilization of the ligands, with mean values of ~3.11 ± 0.50 Å for 3″-HOCBD, ~6.63 ± 0.47 Å for THC, and ~3.27 ± 0.82 Å for CBL. The RMSD variance indicates ligand rearrangements within the binding site. All ligands reach a plateau toward the end of the simulations.

Because ligand RMSD can reflect both ligand displacement and protein rearrangements (all frames were aligned to the protein backbone), we also computed the time series of distances between the center of mass (COM) of each ligand in each frame relative to the COM of each ligand in the equilibrated structures (Figure 4b). The resulting COM displacements were smaller: ~1.25 ± 0.35 Å for 3″-HOCBD, ~1.80 ± 0.35 Å for THC, and ~1.77 ± 0.72 Å for CBL. These results suggest that ligand COMs shift only slightly, and the larger RMSD values primarily reflect structural reorientations within the binding cavity. In

particular, THC shows large RMSD values but small COM displacements, consistent with the ligand flipping within the binding site without leaving it.

We further evaluated the number of contacts between each ligand and the receptor throughout the MD simulations. As shown in Figure 4c, the number of protein atoms within 5 Å of the ligands decreases during the simulation to approximately half of the initial value. Nevertheless, the ligands remain well accommodated within the binding site, as illustrated by the 2D interaction maps in Figure 4d,e. Comparison with the initial docking poses (Supplementary Materials (Figure S1)) shows that largely the same residues are involved in ligand binding, although the nature of their interactions changes during the simulation.

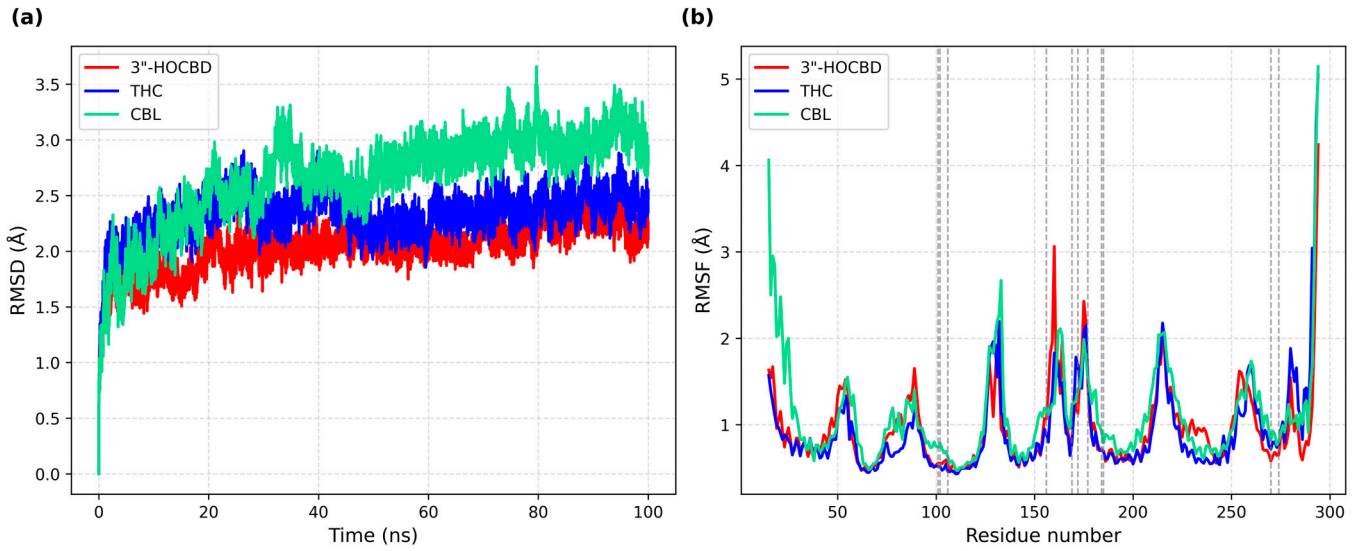


Figure 2. (**a**) RMSD of the protein backbone during the 100 ns MD simulation relative to the equilibrated structure. (**b**) RMSF of protein Cα atoms during the 100 ns MD simulation. The vertical dashed lines mark the ligand binding site residues (TYR101, PHE102, TYR106, ILE156, PHE169, MET172, TRP177, PRO184, LEU185, LEU270 and MET274).

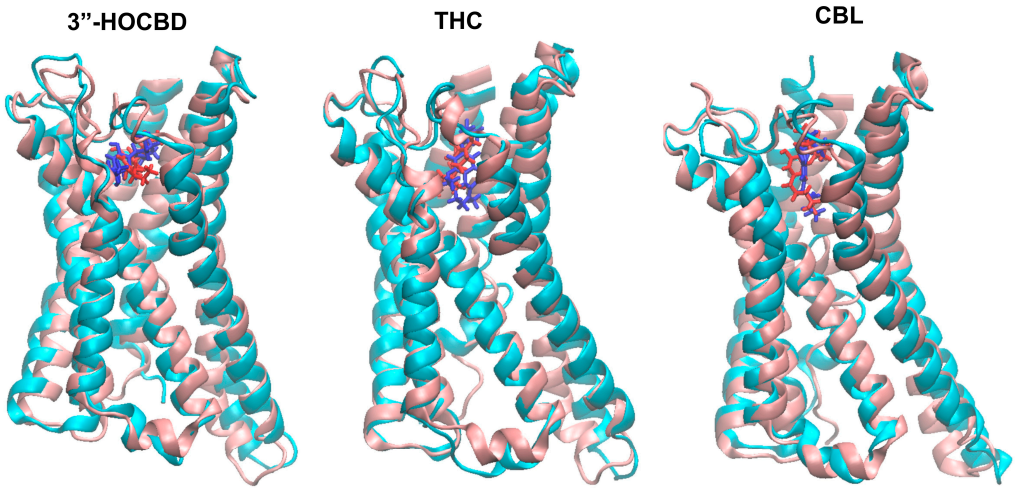


Figure 3. The superimposed structures of GPR55—ligand complexes at the beginning of the MD production run (protein in pink and ligand in red) and at the end of the 100 ns MD simulations (protein in cyan and ligand in blue).

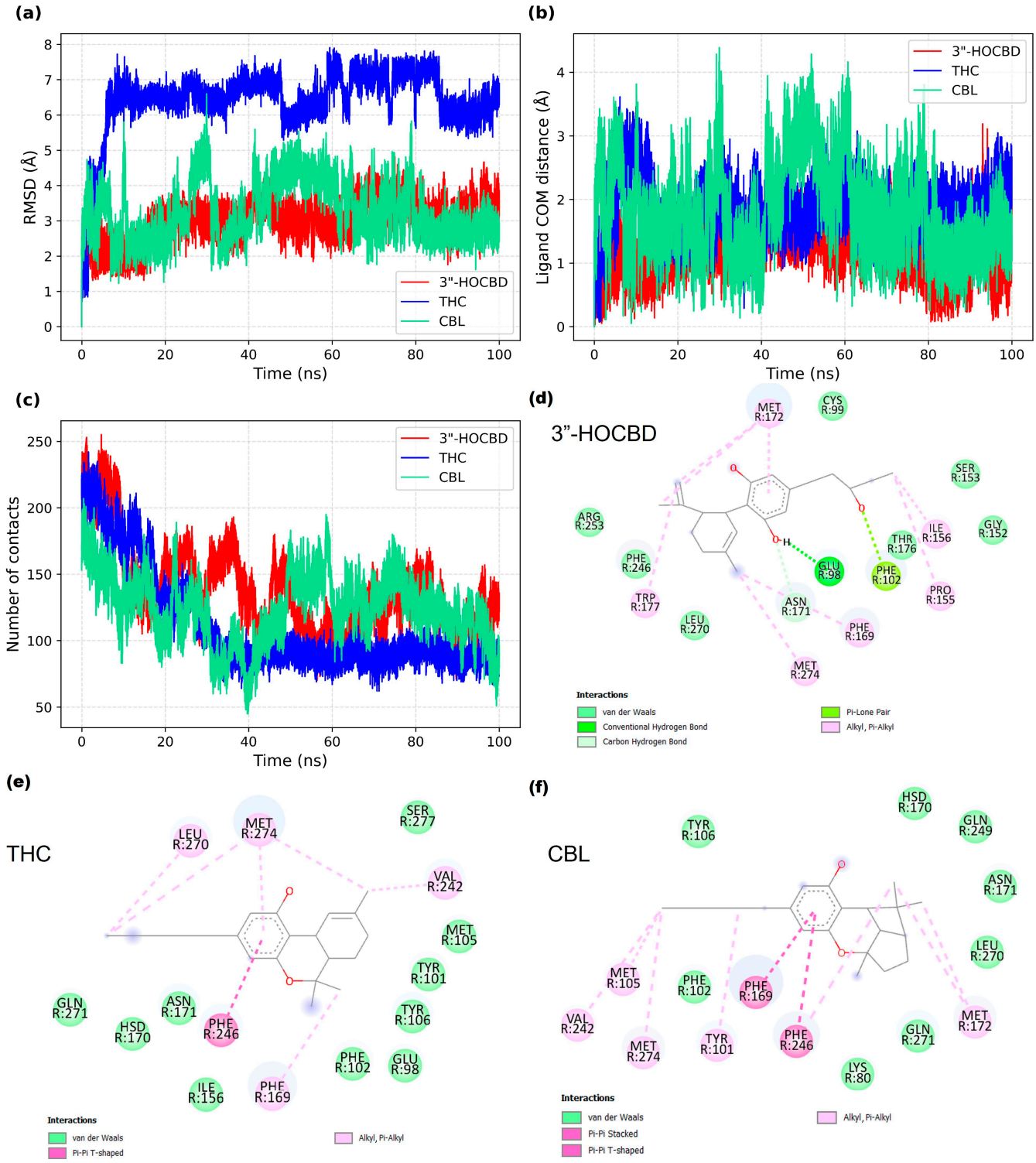


Figure 4. (**a**) RMSD time series of the ligands calculated from the MD trajectories after aligning all frames to the protein backbone. (**b**) Time series of the distance between the ligand center of mass (COM) in each trajectory frame and its COM position in the equilibrated receptor–ligand complex, with all frames aligned to the protein backbone. (**c**) Time series of the number of contacts between the ligand and the protein, defined as the number of protein atoms located within 5 Å of the ligand. (**d**–**f**) 2D interaction maps between the ligands and the protein after 100 ns of MD simulation. The types of interactions in each map are described in the legend. The 2D maps were obtained using Discovery Studio Visualizer [40].

For example, in the 3″-HOCBD complex, GLU98 initially forms van der Waals contacts with the ligand but establishes a hydrogen bond by the end of the simulation. TRP177, which initially engages in van der Waals interactions, shifts to an alkyl interaction, while alkyl interactions involving PRO155, ILE156, PHE169, MET172, and MET274 are maintained in the two conformations (docking pose and the end of the MD simulation). In the case of THC, the ligand initially interacts with PHE246 via van der Waals forces, which evolve into π–π T-shaped interactions during the simulation. Alkyl contacts with PHE169, LEU270, and MET274 are present in both the docking pose and the final conformation after the MD simulation. For CBL, initial van der Waals interactions with PHE246 transition to both π–π stacking and alkyl interactions at the end of the run. Notably, CBL gains new contacts with residues not initially close to the ligand, such as PHE102, MET105, and VAL242, while residues TYR101, LEU270, and MET274 remain involved in interactions in both conformations.

4. Discussion

GPR55 is widely expressed throughout the CNS, with particularly high levels detected in key brain regions involved in motor control, cognition, and sensory integration. These include the basal ganglia, hippocampus, thalamus, and cerebellum, areas implicated in neurodegenerative diseases, epilepsy, and neuropsychiatric disorders [55].

GPR55, along with the other cannabinoid receptors CB1 and CB2, plays an essential role in the CNS. Its activity could be closely related to the behavioral activities of CBD derivatives [56,57]. However, the study by Reyberg and colleagues shows an antagonistic effect of CBD towards GPR55 [58,59]. The regulation of GPR55 expression by CBD contributes to its anti-inflammatory effects, thus having antidepressant effects [60,61]. Shen et al. and Armin et al. study showed behavioral changes in mice with neuropathic pain and depression when administered CBD [60,62]. The findings of the present study support the potential involvement of these derivatives in central nervous system activity. As shown in Table 5, the compounds demonstrate the ability to cross the blood–brain barrier, a key prerequisite for exerting pharmacological effects within the CNS.

Neuroinflammation is recognized as a key process in the pathogenesis of Alzheimer's disease, along with the accumulation of beta-amyloid peptide (Aβ) and the formation of neurofibrillary tangles from hyperphosphorylated tau protein. This is not just a secondary consequence of neuronal damage, but an active factor in the progression of the disease [63]. The studies by Solas et al. and Kurano et al. show the importance of understanding the pharmacology of GPR55, as it is directly linked to neurodegeneration. Modulating the receptor using selective drugs could delay the onset of clinical changes in Alzheimer's dementia [64,65]. The results presented in Table 9 indicate moderately high binding affinities of CBD, CBDV, and CBDP toward the GPR55 receptor, consistent with their previously suggested roles as potential modulators of this receptor. Interestingly, molecular docking analyses also revealed that several other compounds, not initially predicted to interact with GPR55, exhibited even higher binding affinities. This unexpected finding highlights the importance of in silico approaches in uncovering potential novel ligands, expanding the range of compounds that may contribute to the pharmacological modulation of GPR55.

To assess the absorption potential of the compounds, two key parameters were selected: bioavailability and intestinal absorption. These metrics were chosen based on literature reports indicating that CBD and its derivatives exhibit low oral bioavailability, often necessitating specialized pharmaceutical formulations to enhance their absorption and therapeutic efficacy [9,29].

Distribution was evaluated in terms of CNS penetration and blood–brain barrier (BBB) permeability, as these properties are critical for compounds intended to exert pharmacological effects within the CNS. Based on literature data highlighting the psychoactive effects of THC [26], it is expected that CBD derivatives possess the ability to cross the BBB and reach CNS targets. However, despite potential similarities in their mechanisms of action, CBD is considered non-psychoactive according to current research [33,66,67]. The analysis of data in Table 5 reveals that the majority of CBD derivatives exhibit a high predicted probability of crossing the blood–brain barrier (BBB), accompanied by a moderate potential for central nervous system (CNS) penetration. A few exceptions were identified, namely 4″-HOCBD, 5″-HOCBD, 2″-HOCBD, and 3″-HOCBD, which demonstrated slightly reduced BBB permeability, with probability values below 0.8. Despite these exceptions, most derivatives satisfy the criteria for BBB penetration, supporting their candidacy for further investigation as potential modulators of CNS-associated molecular targets.

The metabolism of compounds in the human body is a critical factor in determining their pharmacological activity, as it can lead to either the activation or inactivation of a drug. Metabolic processes primarily occur at the hepatic and, to a lesser extent, renal level [68]. In this analysis, we focus on hepatic metabolism, particularly at the level of cytochrome P450 enzymes. These enzymes, through their various isoforms, play a central role in the biotransformation of compounds—potentially activating them, inhibiting their function, or generating secondary metabolites that may possess different pharmacodynamic or toxicological profiles [29,69,70]. CBD derivatives exhibit a high predicted probability of acting as inhibitors of several major cytochrome P450 isoforms, specifically CYP1A2, CYP2C19, CYP2C9, and CYP3A4. This finding highlights their potential to interfere with the metabolism of concomitantly administered drugs, raising concerns regarding possible drug–drug interactions. Furthermore, the prediction that these derivatives may also serve as substrates for CYP2C9 suggests an additional metabolic pathway through which they could be processed. This dual role as both inhibitors and substrates emphasizes the importance of evaluating their metabolic stability and interaction profiles.

Renal excretion is assessed using models that incorporate the activity of Organic Cation Transporter 2 (OCT2), a key protein involved in the renal clearance of many drugs. These models allow for the prediction of a compound's elimination profile, particularly its optimal excretion time. Certain compounds may act as OCT2 inhibitors, modulate its expression, or interfere with its function, potentially altering drug clearance and contributing to renal toxicity [29,71]. The results indicate that neither CBD nor its derivatives are predicted to inhibit OCT2, suggesting that these compounds may undergo efficient renal elimination. Additionally, the predicted half-life of the CBD derivatives is below 3 hs, a parameter of particular importance for therapeutic evaluation. Short elimination half-lives generally support the avoidance of compound accumulation in systemic circulation, thereby reducing the risk of toxicity. However, this characteristic may also necessitate more frequent dosing to maintain therapeutic efficacy, underscoring the need for careful optimization of dosage regimens in future pharmacological studies.

Toxicity remains a critical concern in drug development and has been the reason for the withdrawal of numerous compounds from the market over the years. Advances in bioinformatics have become essential tools for predicting toxicity at multiple biological levels, enabling early screening for adverse effects. Predictive models now assess parameters such as mutagenicity (AMES test), carcinogenicity, hepatotoxicity, and cardiotoxicity [29]. Cardiotoxicity, in particular, is evaluated based on a compound's potential to inhibit the hERG channel—a cardiac potassium channel crucial for the repolarization phase of the cardiac action potential and the maintenance of normal heart rhythm [72–74]. The predicted toxicity profiles of the CBD derivatives are summarized in Table 8. Overall, the majority of

compounds were classified as safe with respect to AMES mutagenicity, hepatotoxicity, and cardiotoxicity. Nevertheless, data obtained from the DeepPK database [29] suggest that both CBD and several of its hydroxy derivatives may carry a potential risk of cardiotoxicity, primarily through predicted inhibition of the hERG potassium channel. This finding is particularly relevant given the well-established association between hERG blockade and drug-induced QT prolongation, which can lead to severe arrhythmias. Among the series, 10-((4-Aminobutyryl)amino)cannabidiol exhibited the highest cardiotoxic potential, indicating that this derivative may not represent a suitable candidate for further drug development. These results underscore the importance of incorporating early cardiotoxicity screening into the preclinical evaluation of cannabinoid derivatives to ensure safety prior to clinical translation.

In addition to the above predictions, we evaluated the drug-likeness profile of the compounds. All selected CBD derivatives complied with key drug-likeness criteria, including Lipinski's rule of five, as evaluated via the SwissADME platform. The compounds exhibited favorable physicochemical profiles, with molecular weights around 500 Da and acceptable logP values, suggesting promising pharmacokinetic properties [31,33].

Following the prediction that some CBD derivatives could modulate GPR55, molecular docking simulations were used to prove the affinity of these ligands for the receptor. Molecular docking revealed high binding affinities across the tested ligands, with scores ranging from -9.2 to -6.8 kcal/mol. These values indicate a strong thermodynamic feasibility for ligand-receptor interactions. Visualization and interaction analysis using Discovery Studio Visualizer revealed that the majority of the top-scoring ligands docket to a conserved binding site on GPR55. The most frequently involved amino acid residues included—TYR101, PHE102, TYR106, ILE156, PHE169, MET172, TRP177, PRO184, LEU185, LEU270 and MET274 located deep within GPR55 cavity. The recurrence of these residues across different ligands highlights their importance for molecular recognition of CBD derivatives. Previous structural studies also identify these residues as key contributors to hydrophobic interactions with ONO-9710531 (structure 9IYA [75], ML184 (structure 9GE2 [24] 1-palmitoyl-2-lysophosphatidylinositol (LPI) (structure 9GE3 [24]) and L-α-lysophosphatidylinositol (LPI) (structure 8ZX5 [23]).

To evaluate the stability of ligand binding within the receptor cavity, molecular dynamics simulations were performed for the three top-scoring GPR55–ligand complexes, namely those with 3″-hydroxycannabidiol (3″-HOCBD), tetrahydrocannabinol (THC), and cannabipinol (CBL). These ligands were selected from the larger panel of 14 docked compounds based on their favorable docking scores and the diversity of their chemical scaffolds. While all three molecules share a cannabinoid backbone, they differ in the degree of hydroxylation and aromatic substitution, which is expected to influence their conformational flexibility and the interaction patterns with the receptor. 3″-HOCBD possesses an additional hydroxyl group that increases its potential for polar interactions, THC contains a more rigid tricyclic structure, whereas CBL exhibits a distinct arrangement of the aromatic rings due to oxidation of the THC scaffold. The inclusion of these three ligands thus provides a representative overview of how structural diversity among cannabinoid analogs affects their accommodation and stability within the GPR55 binding site during the simulation time.

The MD simulations showed that all ligands remained bound within the same binding cavity throughout the 100 ns production runs, though they adopted distinct orientations within the site. The relatively low COM displacements for all three ligands confirmed that the compounds did not dissociate from the receptor, while the observed RMSD fluctuations (larger in the case of THC) primarily reflected local reorientations rather than large-scale displacements. Among the three, 3″-HOCBD exhibited the lowest RMSD and

COM distance variation, consistent with a more stable binding pose and stronger anchoring within the pocket, likely facilitated by its additional hydroxyl group that allows for stronger polar interactions. In contrast, THC showed higher RMSD values, suggesting increased mobility within the binding site, while CBL induced the largest receptor rearrangements, in agreement with the elevated RMSF values observed for binding site residues. Analysis of protein–ligand contacts further supports these findings. Although the total number of contacts decreased during the simulations, key interactions persisted, and several evolved in nature, from van der Waals to hydrogen bonding or π–π stacking, indicating subtle reorganization of the binding interface rather than ligand dissociation. Such dynamic adaptability is consistent with the plasticity of GPR55′s binding cavity, which appears to accommodate chemically distinct cannabinoid analogs through local structural rearrangements of residues including TYR101, PHE102, TRP177, and MET274. These residues are also involved in accommodating the ligands in the experimentally solved structures of GPR55—ligand complexes, suggesting that they may represent key anchoring points for ligand–receptor recognition and potentially contribute to the pharmacological relevance of structurally diverse cannabinoids [24].

Moreover, the predicted oral bioavailability scores for these derivatives were moderate (0.55), which aligns with literature reports suggesting the need for specialized pharmaceutical formulations to enhance the systemic absorption of CBD-based compounds.

5. Conclusions

This study provides a comprehensive bioinformatics evaluation of CBD derivatives, integrating molecular modeling, pharmacokinetic predictions, and docking studies to assess their potential as modulators of the GPR55 receptor. Our analyses revealed that most compounds exhibit favorable drug-like properties, complying with key drug design criteria such as Lipinski′s rule of five and optimal molecular weight for oral administration. ADMET profiling suggested efficient absorption and renal clearance, with the majority of derivatives predicted to cross the blood–brain barrier, thereby supporting their possible central nervous system activity. Importantly, while most compounds demonstrated acceptable safety profiles with no major risks of mutagenicity or hepatotoxicity, certain hydroxy derivatives and 10-((4-Aminobutyryl)amino)cannabidiol displayed potential cardiotoxicity through hERG inhibition, warranting cautious consideration in further development.

Molecular docking studies confirmed the binding affinities of CBD derivatives toward the GPR55 receptor, consistent with literature reports of their biological activity and also revealing new potential ligands not previously reported. The most favorable binding affinity was obtained for 3″-HOCBD, THC, THCV, CBL, CBC, and 10-((4-Aminobutyryl)amino)cannabidiol. Molecular dynamics simulations were performed to assess the stability of the top-scoring compounds 3″-HOCBD, THC and CBL within the GPR55 binding site. Overall, the simulations suggest that the three ligands maintain stable interactions within the GPR55 binding pocket, with 3″-HOCBD showing the most stable binding, THC exhibiting intrapocket reorientation, and CBL promoting moderate local flexibility of the receptor. These results provide insight into how structural diversity among cannabinoid derivatives influences their accommodation and dynamics within the receptor.

Overall, our results support the hypothesis that CBD derivatives may exert central effects through interactions with GPR55 and related molecular targets, reinforcing their pharmacological relevance in neurological, inflammatory, and oncological conditions. Future studies should include experimental validation to confirm the computational predictions and to better define the therapeutic potential and safety profile of these compounds.

Supplementary Materials: The following supporting information can be downloaded at: https://www.mdpi.com/article/10.3390/pr13103261/s1, Figure S1. 2D interaction maps of ligands with the GPR55 receptor, generated from docking complexes using Discovery Studio Visualizer [40].

Author Contributions: Conceptualization, S.A., M.M., A.-M.P. and C.M. (Catalina Mares); methodology, C.M. (Catalina Mares) and M.M.; software, A.-M.P.; validation, C.M. (Cristina Matanie), M.M., A.-M.P. and S.A.; formal analysis, M.M. and C.M. (Cristina Matanie); investigation, A.-M.P., C.M. (Cristina Matanie), S.A. and C.M. (Catalina Mares); resources, S.A.; data curation, C.M. (Catalina Mares); writing—original draft preparation, C.M. (Catalina Mares) and A.-M.P.; writing—review and editing, M.M. and A.-M.P.; visualization, C.M. (Catalina Mares) and M.M.; supervision, S.A. All authors have read and agreed to the published version of the manuscript.

Funding: This research received no external funding.

Data Availability Statement: The original contributions presented in this study are included in the article. Further inquiries can be directed to the corresponding author.

Acknowledgments: We gratefully acknowledge the Department of Bioinformatics and Structural Biochemistry, Institute of Biochemistry of the Romanian Academy, for granting access to their computing facilities. We especially thank Teodor Asvadur Sulea for his valuable assistance during the computational work. During the preparation of this manuscript, the author(s) used ChatGPT-5 (OpenAI, San Francisco, CA, USA) for drafting assistance, including typing support and grammar checking. The authors have reviewed and edited the output and take full responsibility for the content of this publication.

Conflicts of Interest: The authors declare no conflicts of interest.

Abbreviations

The following abbreviations are used in this manuscript:

CBD	Cannabidiol
THC	Tetrahydrocannabinol
CBC	Cannabichromene
CBDV	Cannabidivarin
CBL	Cannabicyclol
CBDP	Cannabidiphorol
THCV	Tetrahydrocannabivarin
1″-HOCBD	1″-Hydroxycannabidiol
4″-HOCBD	4″-Hydroxycannabidiol
5″-HOCBD	5″-Hydroxycannabidiol
2″-HOCBD	2″-Hydroxycannabidiol
3″-HOCBD	3″-Hydroxycannabidiol
CBDE	5-ethyl-2-[(1R,6R)-3-methyl-6-(1-methylethenyl)-2-cyclohexen-1-yl]-1,3-benzenediol
GPR55	G-protein coupled receptor 55
CNR1	Cannabinoid receptor 1
CNR2	Cannabinoid receptor 2
GLRA1	Glycine receptor subunit alpha-1
MW	Molecular weight
TPSA	Topological polar surface area
LOG P	Coefficient of partition
CNS	Central nervous system
RMSD	Root mean squared deviation
RMSF	Root mean squared fluctuation
COM	Center of mass

References

1. Bonini, S.A.; Premoli, M.; Tambaro, S.; Kumar, A.; Maccarinelli, G.; Memo, M.; Mastinu, A. Cannabis Sativa: A Comprehensive Ethnopharmacological Review of a Medicinal Plant with a Long History. *J. Ethnopharmacol.* **2018**, *227*, 300–315. [CrossRef]
2. Atalay, S.; Jarocka-Karpowicz, I.; Skrzydlewska, E. Antioxidative and Anti-Inflammatory Properties of Cannabidiol. *Antioxidants* **2019**, *9*, 21. [CrossRef]
3. Aran, A.; Harel, M.; Cassuto, H.; Polyansky, L.; Schnapp, A.; Wattad, N.; Shmueli, D.; Golan, D.; Castellanos, F.X. Cannabinoid Treatment for Autism: A Proof-of-Concept Randomized Trial. *Mol. Autism* **2021**, *12*, 6. [CrossRef]
4. McGuire, P.; Robson, P.; Cubala, W.J.; Vasile, D.; Morrison, P.D.; Barron, R.; Taylor, A.; Wright, S. Cannabidiol (CBD) as an Adjunctive Therapy in Schizophrenia: A Multicenter Randomized Controlled Trial. *Am. J. Psychiatry* **2018**, *175*, 225–231. [CrossRef]
5. Wright, M.; Di Ciano, P.; Brands, B. Use of Cannabidiol for the Treatment of Anxiety: A Short Synthesis of Pre-Clinical and Clinical Evidence. *Cannabis Cannabinoid Res.* **2020**, *5*, 191–196. [CrossRef]
6. Schiavon, A.P.; Bonato, J.M.; Milani, H.; Guimarães, F.S.; Weffort de Oliveira, R.M. Influence of Single and Repeated Cannabidiol Administration on Emotional Behavior and Markers of Cell Proliferation and Neurogenesis in Non-Stressed Mice. *Prog. Neuropsychopharmacol. Biol. Psychiatry* **2016**, *64*, 27–34. [CrossRef]
7. Mooko, T.; Bala, A.; Tripathy, S.; Kumar, C.S.; Mahadevappa, C.P.; Chaudhary, S.K.; Matsabisa, M.G.; Cannabis Sativa, L. Flower and Bud Extracts Inhibited In Vitro Cholinesterases and β-Secretase Enzymes Activities: Possible Mechanisms of Cannabis Use in Alzheimer Disease. *Endocr. Metab. Immune Disord. Drug Targets* **2022**, *22*, 297–309. [CrossRef]
8. Pisanti, S.; Malfitano, A.M.; Ciaglia, E.; Lamberti, A.; Ranieri, R.; Cuomo, G.; Abate, M.; Faggiana, G.; Proto, M.C.; Fiore, D.; et al. Cannabidiol: State of the Art and New Challenges for Therapeutic Applications. *Pharmacol. Ther.* **2017**, *175*, 133–150. [CrossRef]
9. Elsaid, S.; Le Foll, B. The Complexity of Pharmacology of Cannabidiol (CBD) and Its Implications in the Treatment of Brain Disorders. *Neuropsychopharmacology* **2020**, *45*, 229–230. [CrossRef]
10. Castillo-Arellano, J.; Canseco-Alba, A.; Cutler, S.J.; León, F. The Polypharmacological Effects of Cannabidiol. *Molecules* **2023**, *28*, 3271. [CrossRef]
11. Millar, S.A.; Stone, N.L.; Yates, A.S.; O'Sullivan, S.E. A Systematic Review on the Pharmacokinetics of Cannabidiol in Humans. *Front. Pharmacol.* **2018**, *9*, 1365. [CrossRef]
12. Lim, S.Y.; Sharan, S.; Woo, S. Model-Based Analysis of Cannabidiol Dose-Exposure Relationship and Bioavailability. *Pharmacother. J. Hum. Human. Pharmacol. Drug Ther.* **2020**, *40*, 291–300. [CrossRef]
13. Taylor, L.; Gidal, B.; Blakey, G.; Tayo, B.; Morrison, G. A Phase I, Randomized, Double-Blind, Placebo-Controlled, Single Ascending Dose, Multiple Dose, and Food Effect Trial of the Safety, Tolerability and Pharmacokinetics of Highly Purified Cannabidiol in Healthy Subjects. *CNS Drugs* **2018**, *32*, 1053–1067. [CrossRef]
14. Nadulski, T.; Pragst, F.; Weinberg, G.; Roser, P.; Schnelle, M.; Fronk, E.-M.; Stadelmann, A.M. Randomized, Double-Blind, Placebo-Controlled Study about the Effects of Cannabidiol (CBD) on the Pharmacokinetics of Delta9-Tetrahydrocannabinol (THC) after Oral Application of THC Verses Standardized Cannabis Extract. *Ther. Drug Monit.* **2005**, *27*, 799–810. [CrossRef]
15. Elsohly, M.A.; Slade, D. Chemical Constituents of Marijuana: The Complex Mixture of Natural Cannabinoids. *Life Sci.* **2005**, *78*, 539–548. [CrossRef]
16. Nader, D.A.; Sanchez, Z.M. Effects of Regular Cannabis Use on Neurocognition, Brain Structure, and Function: A Systematic Review of Findings in Adults. *Am. J. Drug Alcohol. Abus.* **2018**, *44*, 4–18. [CrossRef]
17. Patil, N.; Chandel, V.; Rana, A.; Jain, M.; Kaushik, P. Investigation of Cannabis Sativa Phytochemicals as Anti-Alzheimer's Agents: An In Silico Study. *Plants* **2023**, *12*, 510. [CrossRef]
18. Patil, N.; Patil, K.; Jain, M.; Mohammed, A.; Yadav, A.; Dhanda, P.S.; Kole, C.; Dave, K.; Kaushik, P.; Azhar Abdul Razab, M.K.; et al. A Systematic Study of Molecular Targets of Cannabidiol in Alzheimer's Disease. *J. Alzheimers Dis. Rep.* **2024**, *8*, 1339–1360. [CrossRef]
19. Shen, S.-Y.; Yu, R.; Li, W.; Liang, L.-F.; Han, Q.-Q.; Huang, H.-J.; Li, B.; Xu, S.-F.; Wu, G.-C.; Zhang, Y.-Q.; et al. The Neuroprotective Effects of GPR55 against Hippocampal Neuroinflammation and Impaired Adult Neurogenesis in CSDS Mice. *Neurobiol. Dis.* **2022**, *169*, 105743. [CrossRef]
20. Hill, J.D.; Zuluaga-Ramirez, V.; Gajghate, S.; Winfield, M.; Sriram, U.; Rom, S.; Persidsky, Y. Activation of GPR55 Induces Neuroprotection of Hippocampal Neurogenesis and Immune Responses of Neural Stem Cells Following Chronic, Systemic Inflammation. *Brain Behav. Immun.* **2019**, *76*, 165–181. [CrossRef]
21. Liu, B.; Song, S.; Jones, P.M.; Persaud, S.J. GPR55: From Orphan to Metabolic Regulator? *Pharmacol. Ther.* **2015**, *145*, 35–42. [CrossRef]
22. Marichal-Cancino, B.A.; Fajardo-Valdez, A.; Ruiz-Contreras, A.E.; Mendez-Díaz, M.; Prospero-García, O. Advances in the Physiology of GPR55 in the Central Nervous System. *Curr. Neuropharmacol.* **2017**, *15*, 771–778. [CrossRef]
23. Xia, R.; Yuan, Q.; Wang, N.; Hou, L.; Abe, J.; Song, J.; Ito, Y.; Xu, H.E.; He, Y. Structural Insight into GPR55 Ligand Recognition and G-Protein Coupling. *Cell Res.* **2025**, *35*, 76–79. [CrossRef]

24. Claff, T.; Ebenhoch, R.; Kley, J.T.; Magarkar, A.; Nar, H.; Weichert, D. Structural Basis for Lipid-Mediated Activation of G Protein-Coupled Receptor GPR55. *Nat. Commun.* **2025**, *16*, 1973. [CrossRef] [PubMed]
25. Kim, S.; Chen, J.; Cheng, T.; Gindulyte, A.; He, J.; He, S.; Li, Q.; Shoemaker, B.A.; Thiessen, P.A.; Yu, B.; et al. PubChem in 2021: New Data Content and Improved Web Interfaces. *Nucleic Acids Res.* **2021**, *49*, D1388–D1395. [CrossRef]
26. Cherry, A.L.; Wheeler, M.J.; Mathisova, K.; Di Miceli, M. In Silico Analyses of the Involvement of GPR55, CB1R and TRPV1: Response to THC, Contribution to Temporal Lobe Epilepsy, Structural Modeling and Updated Evolution. *Front. Neuroinform.* **2024**, *18*, 1294939. [CrossRef]
27. Putz, M.V.; Duda-Seiman, C.; Duda-Seiman, D.; Putz, A.-M.; Alexandrescu, I.; Mernea, M.; Avram, S. Chemical Structure-Biological Activity Models for Pharmacophores' 3D-Interactions. *Int. J. Mol. Sci.* **2016**, *17*, 1087. [CrossRef]
28. Dallakyan, S.; Olson, A.J. Small-Molecule Library Screening by Docking with PyRx. In *Chemical Biology: Methods and Protocols*; Hempel, J.E., Williams, C.H., Hong, C.C., Eds.; Springer: New York, NY, USA, 2015; pp. 243–250. ISBN 978-1-4939-2269-7.
29. Myung, Y.; de Sá, A.G.C.; Ascher, D.B. Deep-PK: Deep Learning for Small Molecule Pharmacokinetic and Toxicity Prediction. *Nucleic Acids Res.* **2024**, *52*, W469–W475. [CrossRef]
30. Garisetti, V.; Varughese, R.E.; Anandamurthy, A.; Haribabu, J.; Dasararaju, G. Exploring Potential GPR55 Agonists Using Virtual Screening, Molecular Docking and Dynamics Simulation Studies. *J. Biomol. Struct. Dyn.* **2024**, 1–13. [CrossRef]
31. Lipinski, C.A.; Lombardo, F.; Dominy, B.W.; Feeney, P.J. Experimental and Computational Approaches to Estimate Solubility and Permeability in Drug Discovery and Development Settings. *Adv. Drug Deliv. Rev.* **2001**, *46*, 3–26. [CrossRef]
32. Avram, S.; Mernea, M.; Mihailescu, D.; Duda-Seiman, D.; Duda-Seiman, C. Advanced QSAR Methods Evaluated Polycyclic Aromatic Compounds Duality as Drugs and Inductors in Psychiatric Disorders. *Curr. Org. Chem.* **2013**, *17*, 2880–2890. [CrossRef]
33. Daina, A.; Michielin, O.; Zoete, V. SwissADME: A Free Web Tool to Evaluate Pharmacokinetics, Drug-Likeness and Medicinal Chemistry Friendliness of Small Molecules. *Sci. Rep.* **2017**, *7*, 42717. [CrossRef] [PubMed]
34. Daina, A.; Michielin, O.; Zoete, V. SwissTargetPrediction: Updated Data and New Features for Efficient Prediction of Protein Targets of Small Molecules. *Nucleic Acids Res.* **2019**, *47*, W357–W364. [CrossRef]
35. Meng, E.C.; Goddard, T.D.; Pettersen, E.F.; Couch, G.S.; Pearson, Z.J.; Morris, J.H.; Ferrin, T.E. UCSF ChimeraX: Tools for Structure Building and Analysis. *Protein Sci.* **2023**, *32*, e4792. [CrossRef] [PubMed]
36. Updated Resources for Exploring Experimentally-Determined PDB Structures and Computed Structure Models at the RCSB Protein Data Bank | Nucleic Acids Research | Oxford Academic. Available online: https://academic.oup.com/nar/article/53/D1/D564/7912033?login=false (accessed on 23 July 2025).
37. O'Boyle, N.M.; Banck, M.; James, C.A.; Morley, C.; Vandermeersch, T.; Hutchison, G.R. Open Babel: An Open Chemical Toolbox. *J. Cheminform.* **2011**, *3*, 33. [CrossRef] [PubMed]
38. AutoDock Vina: Improving the Speed and Accuracy of Docking with a New Scoring Function, Efficient Optimization, and Multithreading-Trott-2010-Journal of Computational Chemistry-Wiley Online Library. Available online: https://onlinelibrary.wiley.com/doi/10.1002/jcc.21334 (accessed on 23 July 2025).
39. Citations—Autodock Vina 1.2.0 Documentation. Available online: https://autodock-vina.readthedocs.io/en/latest/citations.html (accessed on 23 November 2021).
40. Dassault Systèmes BIOVIA. *Discovery Studio Visualizer*, Version 17.2.; Dassault Systèmes: San Diego, CA, USA, 2020.
41. Elbegdorj, O.; Westkaemper, R.B.; Zhang, Y. A Homology Modeling Study toward the Understanding of Three-Dimensional Structure and Putative Pharmacological Profile of the G-Protein Coupled Receptor GPR55. *J. Mol. Graph. Model.* **2013**, *39*, 50–60. [CrossRef]
42. Hetényi, C.; van der Spoel, D. Blind Docking of Drug-Sized Compounds to Proteins with up to a Thousand Residues. *FEBS Lett.* **2006**, *580*, 1447–1450. [CrossRef]
43. Phillips, J.C.; Hardy, D.J.; Maia, J.D.C.; Stone, J.E.; Ribeiro, J.V.; Bernardi, R.C.; Buch, R.; Fiorin, G.; Hénin, J.; Jiang, W.; et al. Scalable Molecular Dynamics on CPU and GPU Architectures with NAMD. *J. Chem. Phys.* **2020**, *153*, 044130. [CrossRef]
44. MacKerell, A.D.; Bashford, D.; Bellott, M.; Dunbrack, R.L.; Evanseck, J.D.; Field, M.J.; Fischer, S.; Gao, J.; Guo, H.; Ha, S.; et al. All-Atom Empirical Potential for Molecular Modeling and Dynamics Studies of Proteins. *J. Phys. Chem. B* **1998**, *102*, 3586–3616. [CrossRef]
45. Huang, J.; Rauscher, S.; Nawrocki, G.; Ran, T.; Feig, M.; de Groot, B.L.; Grubmüller, H.; MacKerell, A.D. CHARMM36m: An Improved Force Field for Folded and Intrinsically Disordered Proteins. *Nat. Methods* **2017**, *14*, 71–73. [CrossRef]
46. Klauda, J.B.; Venable, R.M.; Freites, J.A.; O'Connor, J.W.; Tobias, D.J.; Mondragon-Ramirez, C.; Vorobyov, I.; MacKerell, A.D.; Pastor, R.W. Update of the CHARMM All-Atom Additive Force Field for Lipids: Validation on Six Lipid Types. *J. Phys. Chem. B* **2010**, *114*, 7830–7843. [CrossRef] [PubMed]
47. Vanommeslaeghe, K.; Hatcher, E.; Acharya, C.; Kundu, S.; Zhong, S.; Shim, J.; Darian, E.; Guvench, O.; Lopes, P.; Vorobyov, I.; et al. CHARMM General Force Field (CGenFF): A Force Field for Drug-like Molecules Compatible with the CHARMM All-Atom Additive Biological Force Fields. *J. Comput. Chem.* **2010**, *31*, 671–690. [CrossRef]

48. Kim, S.; Lee, J.; Jo, S.; Brooks, C.L.; Lee, H.S.; Im, W. CHARMM-GUI Ligand Reader & Modeler for CHARMM Force Field Generation of Small Molecules. *J. Comput. Chem.* **2017**, *38*, 1879–1886. [CrossRef]
49. Jo, S.; Kim, T.; Iyer, V.G.; Im, W. CHARMM-GUI: A Web-Based Graphical User Interface for CHARMM. *J. Comput. Chem.* **2008**, *29*, 1859–1865. [CrossRef]
50. Wu, E.L.; Cheng, X.; Jo, S.; Rui, H.; Song, K.C.; Dávila-Contreras, E.M.; Qi, Y.; Lee, J.; Monje-Galvan, V.; Venable, R.M.; et al. CHARMM-GUI Membrane Builder Toward Realistic Biological Membrane Simulations. *J. Comput. Chem.* **2014**, *35*, 1997–2004. [CrossRef]
51. Lee, J.; Cheng, X.; Swails, J.M.; Yeom, M.S.; Eastman, P.K.; Lemkul, J.A.; Wei, S.; Buckner, J.; Jeong, J.C.; Qi, Y.; et al. CHARMM-GUI Input Generator for NAMD, GROMACS, AMBER, OpenMM, and CHARMM/OpenMM Simulations Using the CHARMM36 Additive Force Field. *J. Chem. Theory Comput.* **2016**, *12*, 405–413. [CrossRef]
52. Humphrey, W.; Dalke, A.; Schulten, K. VMD: Visual Molecular Dynamics. *J. Mol. Graph.* **1996**, *14*, 33–38. [CrossRef] [PubMed]
53. Avram, S.; Mernea, M.; Limban, C.; Borcan, F.; Chifiriuc, C. Potential Therapeutic Approaches to Alzheimer's Disease By Bioinformatics, Cheminformatics And Predicted Adme-Tox Tools. *Curr. Neuropharmacol.* **2020**, *18*, 696–719. [CrossRef] [PubMed]
54. Avram, S.; Stan, M.S.; Udrea, A.M.; Buiu, C.; Boboc, A.A.; Mernea, M. 3D-ALMOND-QSAR Models to Predict the Antidepressant Effect of Some Natural Compounds. *Pharmaceutics* **2021**, *13*, 1449. [CrossRef]
55. Martínez-Pinilla, E.; Rico, A.J.; Rivas-Santisteban, R.; Lillo, J.; Roda, E.; Navarro, G.; Lanciego, J.L.; Franco, R. Expression of GPR55 and Either Cannabinoid CB1 or CB2 Heteroreceptor Complexes in the Caudate, Putamen, and Accumbens Nuclei of Control, Parkinsonian, and Dyskinetic Non-Human Primates. *Brain Struct. Funct.* **2020**, *225*, 2153–2164. [CrossRef]
56. Miao, Y.; Zhao, F.; Guan, W. A Novel Insight into the Antidepressant Effect of Cannabidiol: Possible Involvement of the 5-HT1A, CB1, GPR55, and PPARγ Receptors. *Int. J. Neuropsychopharmacol.* **2025**, *28*, pyae064. [CrossRef]
57. Oka, S.; Nakajima, K.; Yamashita, A.; Kishimoto, S.; Sugiura, T. Identification of GPR55 as a Lysophosphatidylinositol Receptor. *Biochem. Biophys. Res. Commun.* **2007**, *362*, 928–934. [CrossRef]
58. Ryberg, E.; Larsson, N.; Sjögren, S.; Hjorth, S.; Hermansson, N.-O.; Leonova, J.; Elebring, T.; Nilsson, K.; Drmota, T.; Greasley, P.J. The Orphan Receptor GPR55 Is a Novel Cannabinoid Receptor. *Br. J. Pharmacol.* **2007**, *152*, 1092–1101. [CrossRef]
59. Sun, L.; Apweiler, M.; Normann, C.; Grathwol, C.W.; Hurrle, T.; Gräßle, S.; Jung, N.; Bräse, S.; Fiebich, B.L. Anti-Inflammatory Effects of GPR55 Agonists and Antagonists in LPS-Treated BV2 Microglial Cells. *Pharmaceuticals* **2024**, *17*, 674. [CrossRef] [PubMed]
60. Shen, Z.; Bao, N.; Chen, J.; Tang, M.; Yang, L.; Yang, Y.; Zhang, H.; Han, J.; Yu, P.; Zhang, S.; et al. Neuromolecular and Behavioral Effects of Cannabidiol on Depressive-Associated Behaviors and Neuropathic Pain Conditions in Mice. *Neuropharmacology* **2024**, *261*, 110153. [CrossRef] [PubMed]
61. Jiang, W.; Yu, W.; Tan, Y. Activation of GPR55 Alleviates Neuropathic Pain and Chronic Inflammation. *Biotechnol. Appl. Biochem.* **2025**, *72*, 196–206. [CrossRef]
62. Armin, S.; Muenster, S.; Abood, M.; Benamar, K. GPR55 in the Brain and Chronic Neuropathic Pain. *Behav. Brain Res.* **2021**, *406*, 113248. [CrossRef] [PubMed]
63. Wang, W.-Y.; Tan, M.-S.; Yu, J.-T.; Tan, L. Role of Pro-Inflammatory Cytokines Released from Microglia in Alzheimer's Disease. *Ann. Transl. Med.* **2015**, *3*, 136. [CrossRef]
64. Solas, M.; Francis, P.T.; Franco, R.; Ramirez, M.J. CB2 Receptor and Amyloid Pathology in Frontal Cortex of Alzheimer's Disease Patients. *Neurobiol. Aging* **2013**, *34*, 805–808. [CrossRef]
65. Kurano, M.; Saito, Y.; Uranbileg, B.; Saigusa, D.; Kano, K.; Aoki, J.; Yatomi, Y. Modulations of Bioactive Lipids and Their Receptors in Postmortem Alzheimer's Disease Brains. *Front. Aging Neurosci.* **2022**, *14*, 1066578. [CrossRef]
66. Avram, S.; Milac, A.-L.; Mihailescu, D. 3D-QSAR Study Indicates an Enhancing Effect of Membrane Ions on Psychiatric Drugs Targeting Serotonin Receptor 5-HT1A. *Mol. Biosyst.* **2012**, *8*, 1418–1425. [CrossRef] [PubMed]
67. Avram, S.; Udrea, A.M.; Negrea, A.; Ciopec, M.; Duteanu, N.; Postolache, C.; Duda-Seiman, C.; Duda-Seiman, D.; Shaposhnikov, S. Prevention of Deficit in Neuropsychiatric Disorders through Monitoring of Arsenic and Its Derivatives as Well as Through Bioinformatics and Cheminformatics. *Int. J. Mol. Sci.* **2019**, *20*, 1804. [CrossRef] [PubMed]
68. Geffrey, A.L.; Pollack, S.F.; Bruno, P.L.; Thiele, E.A. Drug-Drug Interaction between Clobazam and Cannabidiol in Children with Refractory Epilepsy. *Epilepsia* **2015**, *56*, 1246–1251. [CrossRef]
69. Beers, J.L.; Fu, D.; Jackson, K.D. Cytochrome P450–Catalyzed Metabolism of Cannabidiol to the Active Metabolite 7-Hydroxy-Cannabidiol. *Drug Metab. Dispos.* **2021**, *49*, 882–891. [CrossRef]
70. Ikezawa, N.; Iwasa, K.; Sato, F. Molecular Cloning and Characterization of CYP80G2, a Cytochrome P450 That Catalyzes an Intramolecular C-C Phenol Coupling of (S)-Reticuline in Magnoflorine Biosynthesis, from Cultured Coptis Japonica Cells. *J. Biol. Chem.* **2008**, *283*, 8810–8821. [CrossRef]
71. Sholler, D.J.; Spindle, T.R.; Cone, E.J.; Goffi, E.; Kuntz, D.; Mitchell, J.M.; Winecker, R.E.; Bigelow, G.E.; Flegel, R.R.; Vandrey, R. Urinary Pharmacokinetic Profile of Cannabidiol (CBD), Δ9-Tetrahydrocannabinol (THC) and Their Metabolites Following Oral and Vaporized CBD and Vaporized CBD-Dominant Cannabis Administration. *J. Anal. Toxicol.* **2021**, *46*, 494–503. [CrossRef]

72. Gunasekaran, S.; Purushothaman, A.; Anju, K. In Silico Assessment of Cannabidiol from Cannabis Sativa as an Antiviral Agent Against Key Shrimp Pathogens in Aquaculture. *J. Fish Dis.* **2025**, e70015. [CrossRef]
73. Dumitrascu, F.; Udrea, A.-M.; Caira, M.R.; Nuta, D.C.; Limban, C.; Chifiriuc, M.C.; Popa, M.; Bleotu, C.; Hanganu, A.; Dumitrescu, D.; et al. In Silico and Experimental Investigation of the Biological Potential of Some Recently Developed Carprofen Derivatives. *Molecules* **2022**, *27*, 2722. [CrossRef] [PubMed]
74. Mareş, C.; Udrea, A.-M.; Şuţan, N.A.; Avram, S. Bioinformatics Tools for the Analysis of Active Compounds Identified in Ranunculaceae Species. *Pharmaceuticals* **2023**, *16*, 842. [CrossRef] [PubMed]
75. Chang, H.; Li, X.; Shen, L.; Ge, X.; Hao, S.; Wu, L.; Liu, S.; Liu, J.; Cherezov, V.; Hua, T. Structure Basis of Ligand Recognition and Activation of GPR55. *Cell Res.* **2025**, *35*, 80–83. [CrossRef]

Disclaimer/Publisher's Note: The statements, opinions and data contained in all publications are solely those of the individual author(s) and contributor(s) and not of MDPI and/or the editor(s). MDPI and/or the editor(s) disclaim responsibility for any injury to people or property resulting from any ideas, methods, instructions or products referred to in the content.